Applied Surface Science 542 (2021) 148633

Contents lists available at ScienceDirect

Applied Surface Science

journal homepage: www.elsevier.com/locate/apsusc

Full Length Article

Rapid, high-efficient and selective removal of cationic dyes from wastewater using hollow polydopamine microcapsules: Isotherm, kinetics, thermodynamics and mechanism

Mengling Feng [a], Shichao Yu [a], Pengchao Wu [a], Zhiwei Wang [a], Shaohua Liu [b], Jianwei Fu [a,*]

[a] School of Materials Science and Engineering, Zhengzhou University, Zhengzhou 450052, China
[b] State Key Laboratory of Precision Spectroscopy & School of Physics and Materials Science, East China Normal University, Shanghai 200241, China

ARTICLE INFO

Keywords:
Polydopamine
Hollow microcapsule
Selective absorption
Dye
Adsorption kinetics

ABSTRACT

Developing new adsorbents with high adsorption capacity, rapid adsorption rate as well as good adsorption selectivity are highly demanded for efficiently purifying organic wastewater. We here reported new hollow polydopamine microcapsules (H-PDA-MCs) synthesized by a facile oxidation self-polymerization of dopamine using iron trioxide (Fe_2O_3) nano-cube as a template and considered as a high-efficiency adsorbent for capturing organic dyes. First, the morphology and microstructure of H-PDA-MCs were investigated through SEM, TEM, FTIR, XRD, N_2 adsorption and Zeta potential. The adsorption performance of H-PDA-MCs was systematically studied. Second, three kinetic models and five isothermal adsorption models were employed to study the adsorption process and the equilibrium adsorption behavior, respectively. Furthermore, the adsorption mechanism was discussed by FTIR, UV and XPS spectra. The results showed that H-PDA-MCs owned good selective adsorption behavior towards cationic dye. At 298.15 K, the maximum adsorption capacity of H-PDA-MCs towards MB was up to 191.55 mg g^{-1} and the adsorption equilibrium time was only 60 min. The adsorption kinetic process was in line with the pseudo-second-order kinetic model, and the adsorption equilibrium data was well described by the Langmuir and Temkin isotherm models. The thermodynamic parameters demonstrated that the adsorption is an endothermic and spontaneous process.

1. Introduction

With the continuous development of industry and technology, water pollution has become one of the most concerned environment problems by society and government in the world [1]. Especially, the water pollution caused by lots of organic dyes receives more attention. Organic dyes are extensively employed in textile, printing, papermaking, food processing and other modern industries for coloring their diversified products, which leads to a large quantity of colored wastewater [2–4]. These dyes are highly toxic and non-biodegradable (some are carcinogenic and even mutagenic); hence the discharge of dyes-containing effluents into water body could severely threaten the ecological balance and human health [5,6]. Thereby, how to effectively remove organic dyes from wastewater is particularly crucial. Up to now, the dye removal strategies include physicochemical and biological treatments [7–9]. Among them, adsorption is considered to be a simple, low-cost, recyclable and high-efficiency technology [10–14]. And the development of various adsorbents has become the core of adsorption research [15]. Until now, however, the reported adsorbents still had some drawbacks (such as low adsorption capacity, slow adsorption kinetics and poor adsorption selectivity) in their real applications [16–19].

Recently, the researches on micro/nano-scale functionalized polymers have aroused much interest in many application fields, especially in adsorption. As a kind of potential adsorbents, such polymer materials own distinct structural advantages like adjustable chemical structure, abundant functional groups, large specific surface area (SSA) and controllable morphology [18,20]. Generally, the large SSA and abundant functional groups can render adsorbents more adsorption active sites, and the specific functional groups can effectively interact with the target molecules or ions, which greatly increases the adsorption efficiency of adsorbents [21–23]. For example, Xin et al. prepared polypyrrole nanofibers to remove methyl orange (MO) from aqueous solution and the adsorption capacity and the adsorption equilibrium time were 169.55 mg g^{-1} and 120 min, respectively [24]. Chen et al.

* Corresponding author at: School of Materials Science and Engineering, Zhengzhou University, 75 Daxue Road, Zhengzhou 450052, China.
E-mail address: jwfu@zzu.edu.cn (J. Fu).

https://doi.org/10.1016/j.apsusc.2020.148633
Received 8 October 2020; Received in revised form 13 November 2020; Accepted 27 November 2020
Available online 3 December 2020
0169-4332/© 2020 Elsevier B.V. All rights reserved.

used poly(cyclotriphosphazene-co-4,4′-sulfonyldiphenol) nanospheres to remove MB, and the adsorption capacity and the equilibrium time were 20 mg g^{-1} and 420 min, respectively [25]. Though in these studies, considerable progress has been made in terms of improving the adsorption capacity of adsorbents, the slow adsorption rate and poor adsorption selectivity still fail to meet the practical application. Constructing suitable polymer-based adsorbents with unique microstructure might be a good strategy to solve the above problems [20,26]. Polydopamine (PDA) is a typical polymer easily obtained by oxide polymerization of dopamine (DA) at room temperature in alkaline and aerobic environment. It has multiple functional groups such as catechol, amine and imine, which make PDA own potential applications in the fields of chemistry, biology, medicine and materials science [27,28]. More recently, it has been widely reported that PDA could facilely adhere to various substrates through in situ self-polymerization of DA and without the need for sophisticated equipment and harsh reaction conditions [29,30]. Based on these features, many PDA-based adsorption materials have been developed for cleaning the wastewater. Liu et al. used hierarchical porous PU@PDA@MSNs sponge to remove Pb^{2+} ions from aqueous solution, and its adsorption capacity and equilibrium time were 104.2 mg g^{-1} and 800 min, respectively [31]. Xu et al. used magnetically separable h-Fe_3O_4@Au/polydopamine nanosphere with a hollow interior to absorb U(VI), and its adsorption capacity and equilibrium time were 82.9 mg g^{-1} and 120 min, respectively [32]. Therefore, based on the above mechanisms and examples, we guess that the polymer PDA with unique microstructure, as a promising high-efficiency adsorbent candidate, has huge advantages and great potential for use in wastewater treatment.

In our previous study, we synthesized solid PDA microspheres by spontaneous oxidation polymerization of DA at room temperature and investigated their adsorption behavior towards MB [33], and the adsorption capacity and adsorption equilibrium time were 90.7 mg g^{-1} and 80 min at 25 °C, respectively. Hollow capsule particles have attracted much attention due to their low density, high surface volume ratio, excellent surface permeability, remarkable loading capacity and good morphology control. Therefore, in this study, with the aim to further increase the adsorption capacity, shorten the adsorption process and evaluate the adsorption selectivity of PDA towards organic dyes, new hollow PDA microcapsules (H-PDA-MCs) with high SSA were facilely constructed through coating PDA onto the surface of Fe_2O_3 nano-cube to generate core@shell structured Fe_2O_3@PDA hybrid and subsequently removing the hard template Fe_2O_3 nano-cube. The resultant H-PDA-MCs have hollow structure and porous channels in their shell layer, which make them exhibit high adsorption amount, fast adsorption rate and good adsorption selectivity towards cationic dye (MB). Meanwhile, we systematically investigated the effects of diversified factors including initial dye concentration, temperature and solution pH on dye adsorption. Moreover, we also comprehensively evaluated the adsorption thermodynamics, the adsorption kinetics as well as the possible selective adsorption mechanism of H-PDA-MCs towards cationic dye. These studies proved that H-PDA-MCs might be a high-efficient and selective adsorbent for cleaning organic wastewater.

2. Experimental section

2.1. Materials

Dopamine hydrochloride, methyl orange (MO), neutral red (NR), and methyl blue (MB) were analytical reagent and bought from Tianjin Kermel Chemical Reagent CO., Ltd. The tris(hydroxymethyl)aminomethane hydrochloride buffer solution (Tris-buffer), HCl and NaOH were purchased from Sinaopharm Chemical Reagent Co., Ltd.

2.2. Preparation of H-PDA-MCs

The preparation of H-PDA-MCs is based on a hard template mechanism as follows. First, α-Fe_2O_3 nano-cube as hard template was synthesized by a facile co-precipitation method [34]. Second, 665 mL Tris-buffer and 80 mg α-Fe_2O_3 nano-cubes were mixed evenly using the ultrasonic cleaning machine. After 5 min, at room temperature, 40 mg DA was put into the aforementioned solution and the reaction was carried out under aerobic atmosphere and a slow magnetic stirring condition for 24 h. The resulting product (named as Fe_2O_3@PDA) was gathered by centrifugation. Then the deionized water and ethanol were used to wash the above product three times, respectively. Third, the Fe_2O_3@PDA hybrid was etched by 4 M hydrochloric acid for 14 h at 318.15 K to remove Fe_2O_3 core. Finally, the resultant samples were collected by high-speed centrifugation, rinsed using the de-ionized water and dried at 65 °C overnight to obtain hollow PDA microcapsules, namely H-PDA-MCs.

2.3. Batch adsorption experiments

Using MB as a model organic dye, a series of batch adsorption experiments were performed on a TQZ-312 platform incubator with shaking speed of 120 rpm and controllable operating temperature. The adsorption kinetics experiment was performed at 298.15 K, and 20.0 mg of H-PDA-MCs was put into a conical flask with 80 mL of freshly prepared MB solution (the initial concentration was 70 mg L^{-1}). Then, at the different intervals (2, 4, 11, 16, 21, 26, 31, 36, 41, 46, 56, 71, 86, 106, 121, 141, 176, 246, 311 and 412 min), the supernatant was taken out and the concentrations of MB left in the supernatant was calculated by UV–VIS spectrometry. Finally, the adsorption capacity of H-PDA-MCs at a given time was obtained by the following formula:

$$q_t = (C_0 - C_t)V/m \tag{1}$$

where q_t (mg g^{-1}) is the adsorption capacity at a given time, C_0 (mg L^{-1}) is the initial concentration of MB, C_t (mg L^{-1}) represents MB concentration at a given time, V (L) is the solution volume, and m (g) refers to the mass of adsorbent.

To clarify the influence of the initial concentration of organic dyes on adsorption performance of H-PDA-MCs, 5.0 mg of H-PDA-MCs was put into 50 mL of conical flask containing 20 mL of MB solution (the dye concentration was 50, 70, 100, 150, 200 mg L^{-1} respectively). Thereafter, the above five conical bottles were placed in the above shaking incubator at 298.15 K and shaken for 60 min to thoroughly reach adsorption equilibrium. The influence of temperature was evaluated using 70 mg L^{-1} of MB solution and different temperature conditions (288.15, 293.15, 298.15, 303.15 K). By adding 0.1 M NaOH or 0.1 M HCl solution, the initial pH value of MB solution was adjusted to 2–11, and the influence of the initial solution pH was explored. To understand the effect of the dye types on adsorption performance and explore the selective adsorption mechanism of H-PDA-MCs, MO, NR and MB were selected as representative anion dye, neutral dye and cationic dye, respectively. Then q_e (the adsorption quantity at equilibrium, mg g^{-1}) and R (removal efficiency of dyes, %) were calculated according to the following formulas:

$$q_e = V\,(C_0 - C_e)\,/\,m \tag{2}$$

$$R = 100\,(C_0 - C_t)\,/\,C_0 \tag{3}$$

where C_e (mg L^{-1}) represents the residual dye concentration at adsorption equilibrium.

To explore the isothermal property, 5.0 mg of H-PDA-MCs were put into five MB solution with different initial concentrations (50, 70, 100, 150 and 200 mg L^{-1}) and kept at 293.15, 298.15, 303.15 K for 60 min, respectively.

2.4. Regeneration study

Desorption experiments were performed by immersing the dye-

adsorbed H-PDA-MCs into HCl solution (1 M), and the suspension was sonicated in an ultrasonic bath (50 W) for 60 min. Whereafter, the H-PDA-MCs adsorbent was collected by centrifugation and washed with the HCl solution (1 M), de-ionized water and anhydrous ethanol for 3 times respectively, and dried at 65 °C overnight. Finally, a new round of adsorption experiment was carried out with the recycled adsorbent.

2.5. Material characterization

The morphologies of Fe_2O_3@PDA and H-PDA-MCs were examined by scanning electron microscopy (SEM, JEOL JSM-7401F) and transmission scanning microscope (TEM, JEOL JEM-100CX). The functional groups of DA, MB, Fe_2O_3@PDA, H-PDA-MCs, MB-H-PDA-MCs (MB absorbed by H-PDA-MCs) were ascertained by the Fourier transform infrared (FTIR, Perkin-Elmer paragon 1000) spectroscopy. X-ray diffractometer (XRD, Rigaku D/M ax 2550) was applied to confirm the phase structure of Fe_2O_3@PDA and H-PDA-MCs. The SSA and pore diameter distribution of H-PDA-MCs were measured by N_2 adsorption at 77 K on a Micromeritics ASAP 2020 analyzer. The absorbance of a specific dye remaining in the solution at its maximum absorption wavelength can be ascertained by UV–VIS spectroscopy (Shanghai, 752 N), and then the concentration of residual dye can be calculated. The pH meter (Mettler Toledo Co., Ltd., Shanghai) was applied to determine the pH of the dye solution. The charge characteristics of the H-PDA-MCS surface were determined by Zeta potential analysis (Malvern Zetasizer Nano ZS90). The surface chemical composition and elemental status on H-PDA-MCs and H-PDA-MCs-MB were measured by X-ray photoelectron spectroscopy (XPS, Escalab 250XI).

3. Result and discussion

3.1. Preparation and characterization of materials

Fig. 1 illustrates the preparation process of H-PDA-MCs. Firstly, α-Fe_2O_3 nano-cubes were synthesized based on a previously reported method [34]. Then, using α-Fe_2O_3 nano-cubes as hard template, the core@shell structured Fe_2O_3@PDA hybrids were prepared through in-situ oxidation polymerization of dopamine monomer on the surface of α-Fe_2O_3 nano-cubes at room temperature. Finally, the H-PDA-MCs were obtained as soon as the core materials α-Fe_2O_3 nano-cubes were removed by acid-etching.

The morphology and structure of as-prepared samples are revealed by SEM and TEM. From Fig. 2a, it can be seen that the obtained α-Fe_2O_3 presents a nano-cube morphology with diameter of about 380 nm, similar to the previous report [34]. In Fig. 2b, the obtained Fe_2O_3@PDA hybrids show a nearly spherical profile with diameter of about 500 nm, indicating that α-Fe_2O_3 nano-cubes were well encapsulated by a PDA coating. The above results can be confirmed by TEM characterizations, as shown in Fig. 2d and e. Especially in Fig. 2e, the core@shell structure of Fe_2O_3@PDA hybrids can be clearly observed, where the PDA shell exhibits a relatively lighter contrast and owns a thickness of about 61 nm. Of note, no free α-Fe_2O_3 nano-cubes can be found in the TEM and SEM images, suggesting that the PDA coating is highly effective for wrapping α-Fe_2O_3. Fig. 2c displays the typical SEM image of H-PDA-MCs. Obviously, after removing core materials α-Fe_2O_3, the obtained H-PDA-MCs exhibit a hollow structure, which can be confirmed by TEM characterization (Fig. 2f). Noticeably, the structural collapse could be observed on some hollow PDA microcapsules, which is reasonable considering of the soft matter feature of PDA as a kind of organic polymer. Moreover, from Fig. 2f, the wall thickness of H-PDA-MCs is evaluated to be about 71 nm, which is larger than that of PDA coating in the Fe_2O_3@PDA hybrids. It means that the hollow PDA microcapsules as potential adsorbent have better swelling property, which benefits to fast mass transfer in the subsequent application of removing organic dyes from aqueous solution. Additionally, Fig. 2g–j depict the elemental mapping image of H-PDA-MCs. Evidently, C, O and N elements are uniformly distributed in the matrix of hollow polymer, indicating the successful fabrication of hollow PDA microcapsule.

Fig. 3a shows the FTIR spectrum contrast of DA and H-PDA-MCs. In the infrared spectrum of DA, there are many narrow and intense absorption peaks, which are typical of small molecules. However, from the infrared spectrum of H-PDA-MCs, we only observe a few strong absorption peaks [12]. Typically, the characteristic peak at 3373 cm^{-1} is related to the stretching vibration of phenolic O-H and N-H. The characteristic peak at 1611 cm^{-1} is ascribed to the bending vibration of N-H and the stretching vibration of the aromatic ring. And the characteristic peaks at 1511 cm^{-1} should be the shearing vibration of N-H in amine or imine groups. Meanwhile, the characteristic peaks corresponding to the bending vibration and stretching vibration of phenolic C-O-H can be found at 1389 cm^{-1} and 1281 cm^{-1}, respectively. The characteristic peaks corresponding to C-O vibration can be observed at 1122 cm^{-1}. The above peak information indicates that the H-PDA-MCs has been

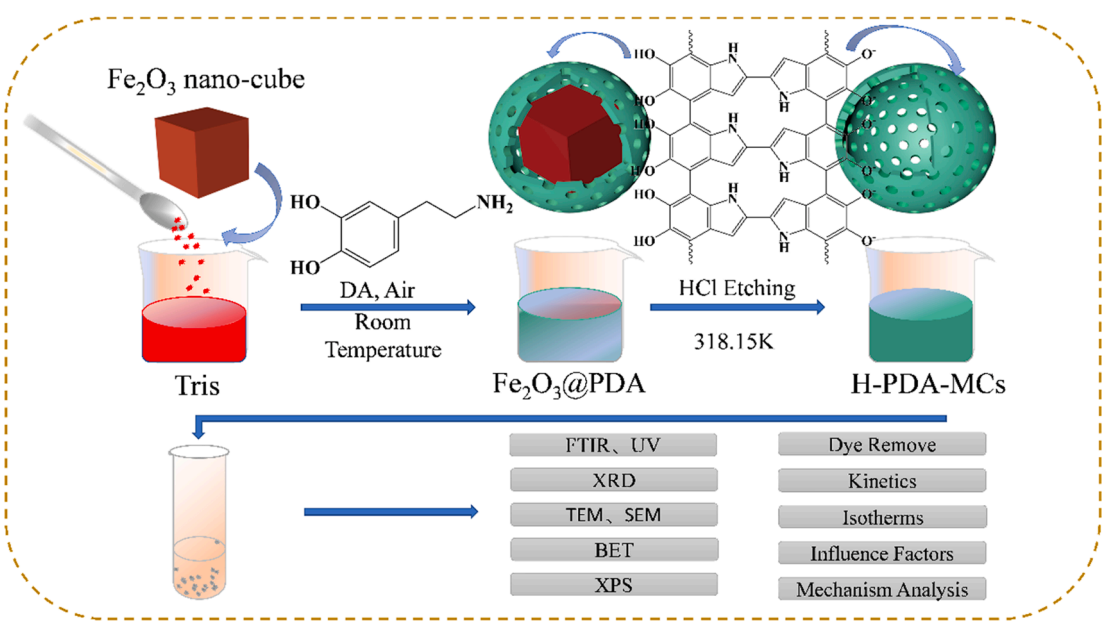

Fig. 1. Synthesis and characterization of H-PDA-MCs.

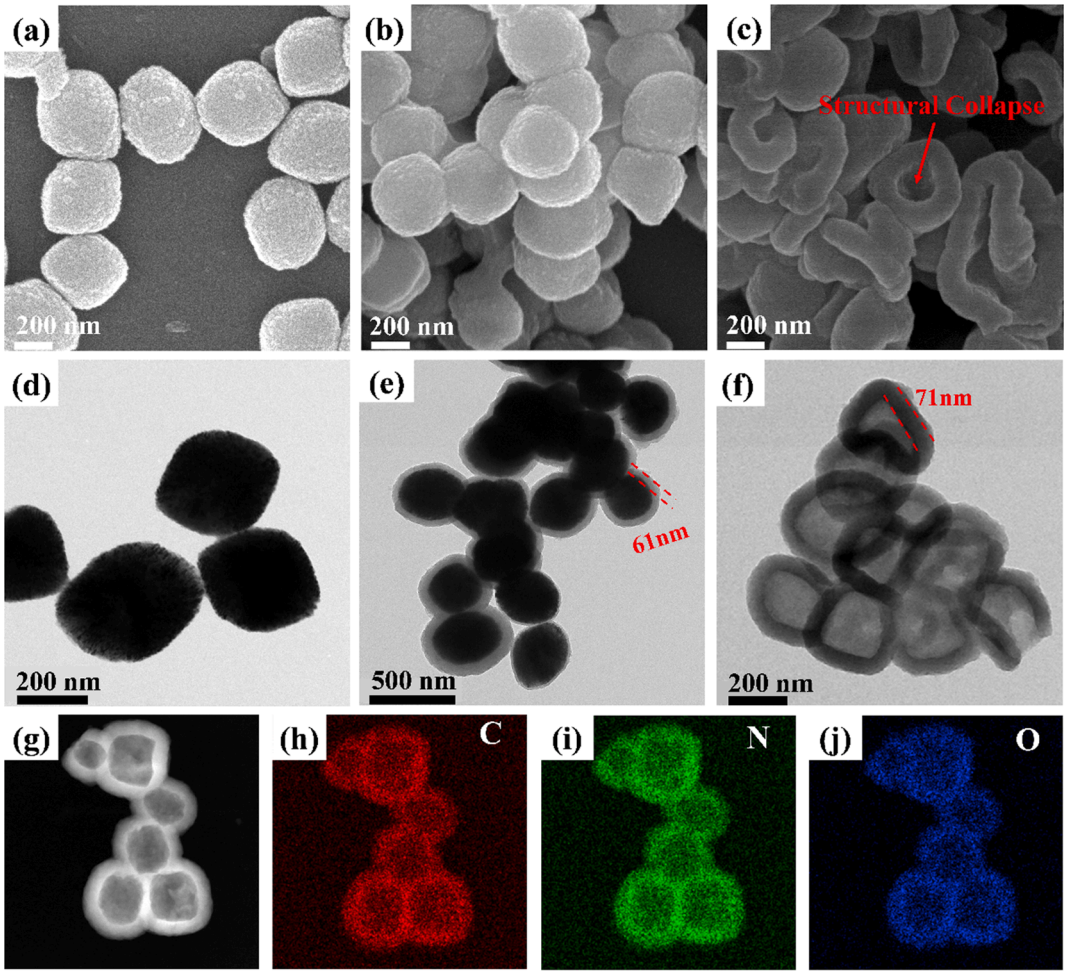

Fig. 2. (a–c) SEM images of Fe_2O_3, Fe_2O_3@PDA and H-PDA-MCs. (d–f) TEM images of Fe_2O_3, Fe_2O_3@PDA and H-PDA-MCs. (g–j) Elemental mapping of H-PDA-MCs.

successfully synthesized by oxidation polymerization of DA and its structure was not damaged under acid etching conditions. And Fig. 1 displays the schematic chemical structure of PDA. Of note, the H-PDA-MCs is rich in a great number of oxygen-containing functional groups, nitrogen-containing functional groups and aromatic rings [35–37], which could be helpful to enhance the interaction between PDA and organic dyes through electrostatic force, hydrogen bond and π-π stacking.

Fig. 3b displays the representative XRD patterns of H-PDA-MCs, Fe_2O_3@PDA and Fe_2O_3 in the range of $2\theta = 10–70°$. It is found that the crystal diffraction peak of Fe_2O_3 nano-cube is in good agreement with that of Fe_2O_3 (JCPDS # 89-0597) [34]. In the XRD pattern of Fe_2O_3@PDA hybrids, the diffraction peak related to Fe_2O_3 still exists but the peak intensity is obviously reduced, which suggested that the Fe_2O_3 nano-cube was well wrapped by PDA. After acid etching, the obtained H-PDA-MCs only presents a wide diffraction peak ($2\theta = 20–25°$) in its XRD pattern, which is typical of amorphous polymer PDA. This indicated that the hard template Fe_2O_3 nano-cubes have been completely removed by acid treatment [32].

Fig. 3c and d show the N_2 adsorption–desorption isotherms and the pore size distribution curves of Fe_2O_3@PDA and H-PDA-MCs at 77 K. According to the normative BET method, the SSA of Fe_2O_3@PDA and H-PDA-MCs are calculated to be approximate 7.11 $m^2\,g^{-1}$ and 24.4 $m^2\,g^{-1}$, respectively. Obviously, the removal of Fe_2O_3 core in Fe_2O_3@PDA hybrids resulted in a sharp increase in the SSA of as-obtained H-PDA-MCs. Such a high SAA can furnish plenty of adsorption sites for adsorbents, which is conducive to the mutual contact between adsorbent (H-PDA-MCs) and adsorbate molecules and achieve the purpose of high-efficient adsorption [37]. Meanwhile, from the N_2 adsorption–desorption curves of H-PDA-MCs we can notice that there is an obvious hysteresis loop at a relative pressure of $P/P^0 > 0.4$ and a sharp increase in nitrogen uptake at a higher relative pressure ($P/P^0 > 0.9$), which suggests the coexistence of well-developed mesopores and macropores [38]. This result can be confirmed by the pore size distribution of H-PDA-MCs (Fig. 3d). We can speculate that the macropores in H-PDA-MCs is mainly related to the hollow structure of the PDA microcapsules and the mesopores might originate from the non-adequately cross-linked PDA shell. Of note, the mesopores could provide rapid diffusion channel for adsorbate molecules and the macrospores could fill adsorbates, which would benefit to greatly enhance the adsorption capacity and adsorption rate of H-PDA-MCs towards organic dyes in the real application.

3.2. Batch adsorption experiment

3.2.1. Effect of initial concentrations

Fig. 4a shows the effect of initial MB concentration on the adsorption capacity of H-PDA-MCs at 298.15 K. Clearly, as the initial MB concentration increases, the adsorption quantities of H-PDA-MCs present a tendency of dramatic increase at the low concentration and then slow increase at the high concentration. For the adsorbent H-PDA-MCs with a fixed mass, its surface adsorption sites can effectively contact with nearly all the MB molecules at the lower MB concentration. However, the available adsorption sites on the H-PDA-MCs could attain saturation at the higher MB concentration. Therefore, the removal efficiency for the given adsorbent H-PDA-MCs exhibits a decline trend together with the increase of the initial MB concentration, as displayed in Fig. 4b. Of note,

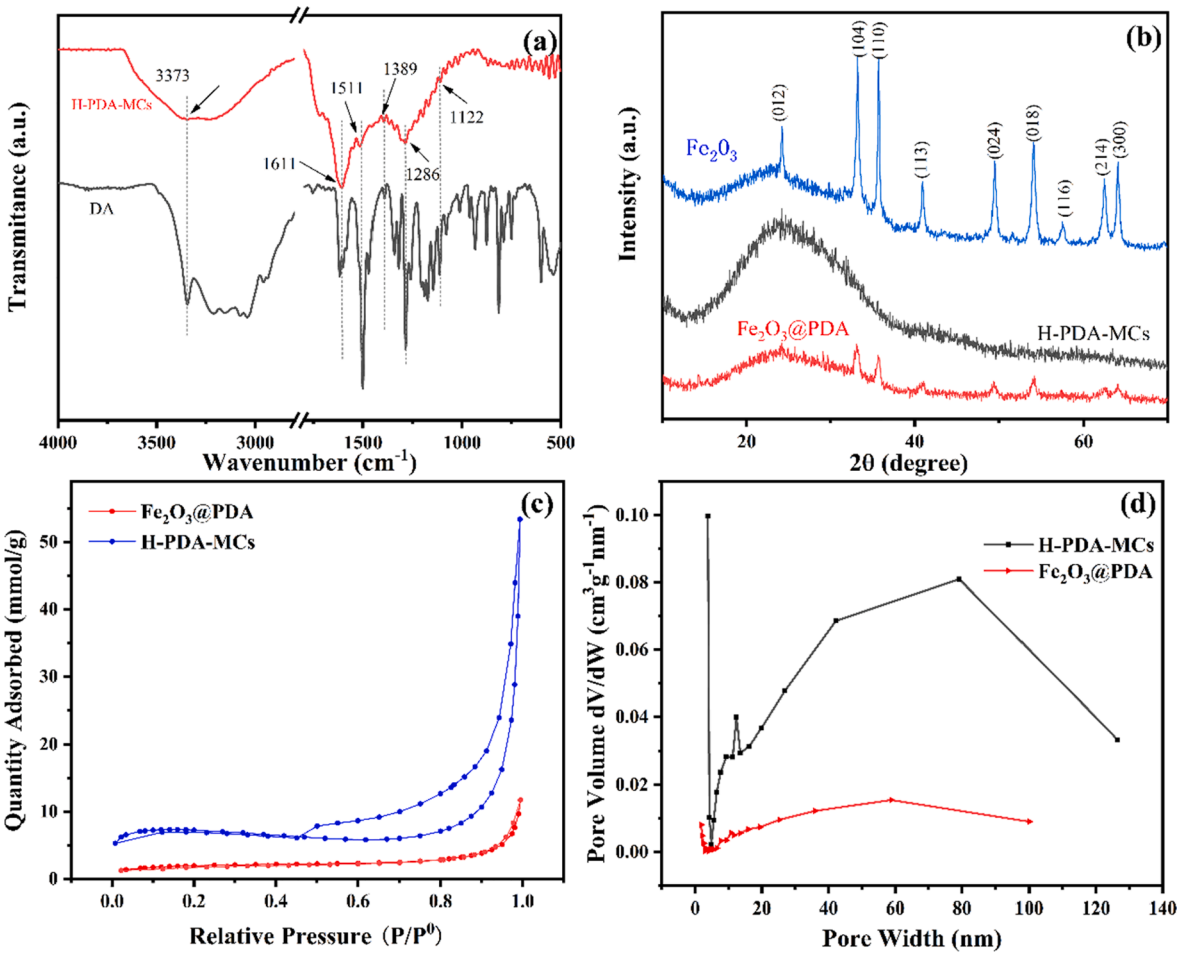

Fig. 3. (a) FT-IR spectra of DA and H-PDA-MCs. (b) XRD patterns of H-PDA-MCs, Fe_2O_3 and PDA@Fe_2O_3. (c–d) Nitrogen adsorption–desorption isotherms (c) and the corresponding pore size distribution curves (d) of H-PDA-MCs and Fe_2O_3@PDA.

when the initial MB concentration is 50 mg L^{-1}, the removal efficiency could be up to 82% with adsorption capacity of 164.41 mg g^{-1}, suggesting the H-PDA-MCs are a high-efficiency adsorbent for MB removal from aqueous solution. In addition, we also investigated the effect of initial MB concentration on the adsorptive performance of H-PDA-MCs at other two temperatures (293.15 K and 303.15 K), and the laws of two group curves are basically the same as that measured at 298.15 K, as shown in Fig. 4c.

3.2.2. *Effect of temperature*

To investigate the influence of temperature on the adsorptive performance of the H-PDA-MCs, a series of adsorption experiments were conducted for the removal of 70 mg L^{-1} MB dye using 20 mg H-PDA-MCs at different temperatures. As displayed in Fig. 4d, when the system temperature increases within the range of 15–35 °C, the adsorption capacity of H-PDA-MCs increases significantly, implying MB adsorption onto the H-PDA-MCs is endothermic. Similar results can also be reflected from Fig. 4c. Of note, the adsorption capacity of H-PDA-MCs at 35 °C attained the maximum value of 185 mg g^{-1}, which revealed that high temperature favored the MB adsorption. The reason can be explained that high temperature can cause an increase in dye molecule mobility and a decrease in solution viscosity, which may provide a greater possibility for capturing more MB molecule by H-PDA-MCs [37].

3.2.3. *Effect of initial solution pH*

It is well known that the initial solution pH value is one of the key factors to be considered in performing adsorption experiments. In this work, the influence of initial solution pH on MB adsorption by H-PDA-MCs was checked by verifying the pH from 2 to 10. As shown in Fig. 4e, when the initial solution pH increases at the investigated range, the adsorption capacity of H-PDA-MCs towards target dye MB shows an upward trend. Especially, the adsorption amount was up to 277.93 mg g^{-1} together with removal efficiency of 99.26% when the pH value reaches 10, indicating that solution pH is a key parameter of influencing the MB adsorption performance and the alkaline environment is more conducive to MB adsorption onto H-PDA-MCs. To clarify the reason, the zeta potential of H-PDA-MCs, which can reflect the surface charge status of adsorbent, was checked and the result was shown in Fig. 4f. The surface of H-PDA-MCs is obviously in a state of zero charge when the solution pH value is about 3. Namely, the point of zero charge (pH_{pzc}) of H-PDA-MCs is approximately 3. When the solution pH value is less than 3, the H-PDA-MCs are positively charged on its surface. In such acidic environment, the electrostatic repulsion could occur between positively charged H-PDA-MCs adsorbent and cationic dye MB, causing a low adsorption capacity. When the solution pH value is over pH_{pzc}, the surface of the adsorbent is in a state of negative charge, which is on account of the deprotonation of the phenol group in H-PDA-MCs. Consequently, there is an electrostatic attraction between negatively charged H-PDA-MCs adsorbent and cationic dye MB, thus promoting the uptake of H-PDA-MCs towards MB dye. Moreover, this uptake interaction could be strengthened with the increase of pH values. Of note, at the zero potential point, the adsorption amount of H-PDA-MCs towards MB still reached 117 mg g^{-1}, which should be ascribed to π-π stacking interaction and hydrogen bonding interaction between H-PDA-MCs and MB [12,24,37,39] and the detailed discussion is seen in the following adsorption mechanism part.

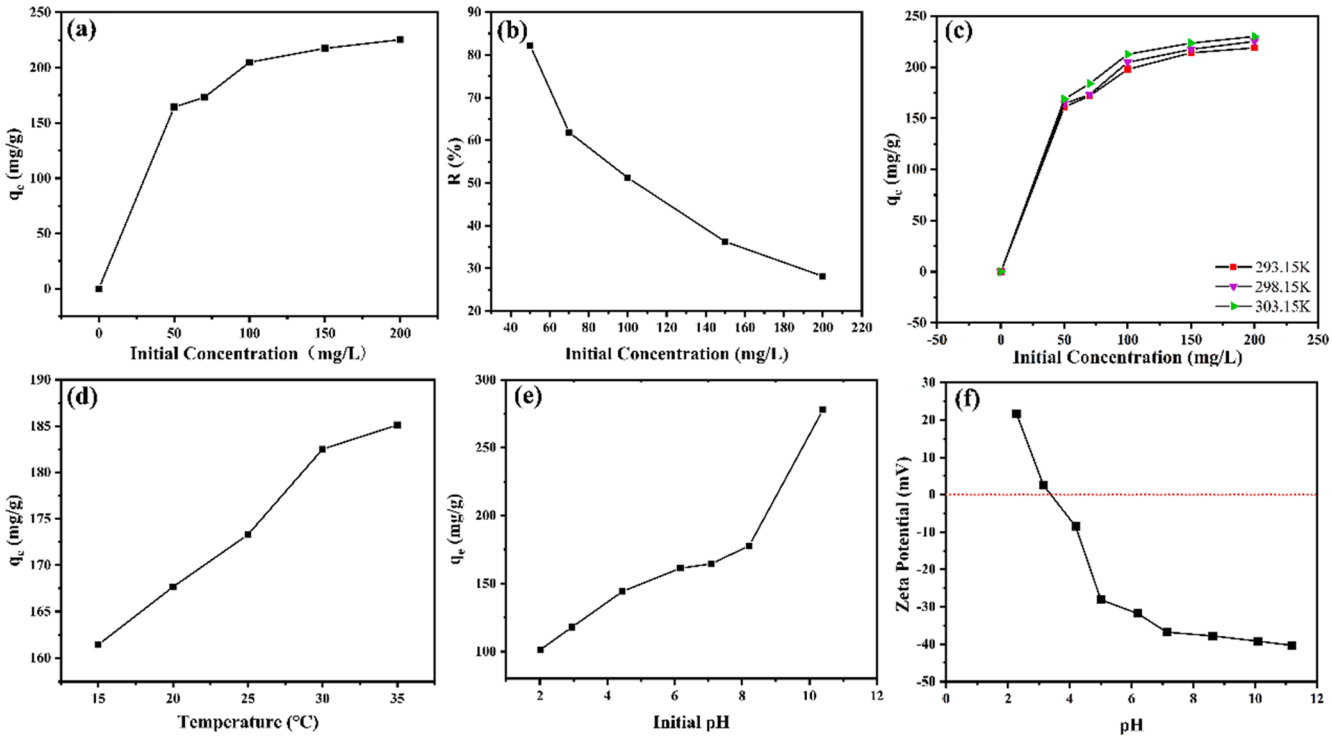

Fig. 4. (a–b) Effects of initial concentrations on the adsorption of MB onto the H-PDA-MCs. (c) Effects of initial concentrations on the adsorption of MB onto the H-PDA-MCs at different temperature. (d) Effects of temperature on the adsorption of MB onto the H-PDA-MCs. (e) Effects of initial pH on the adsorption of MB dyes. (f) Zeta potential of the H-PDA-MCs at different pH values.

3.2.4. Selective adsorption and regeneration performance

To check the adsorption selectivity of H-PDA-MCs towards target dye, three representative dyes, anionic dye methylene orange (MO), neutral dye neutral red (NR) and cationic dye MB, were selected to perform the contrast experiments. The colors of dye solution before and after adsorption were recorded by photographing. Fig. 5a displays the results of adsorption experiments of MO, NR and MB respectively in a single dye solution system. It can be found from the digital photos that the color of MO dye solution hardly changed before and after adsorption, indicating that the adsorbent H-PDA-MCs has a poor adsorption capacity towards anionic dye MO. Relatively, H-PDA-MCs possess a better adsorption capacity for neutral dye NR and cationic dye MB,

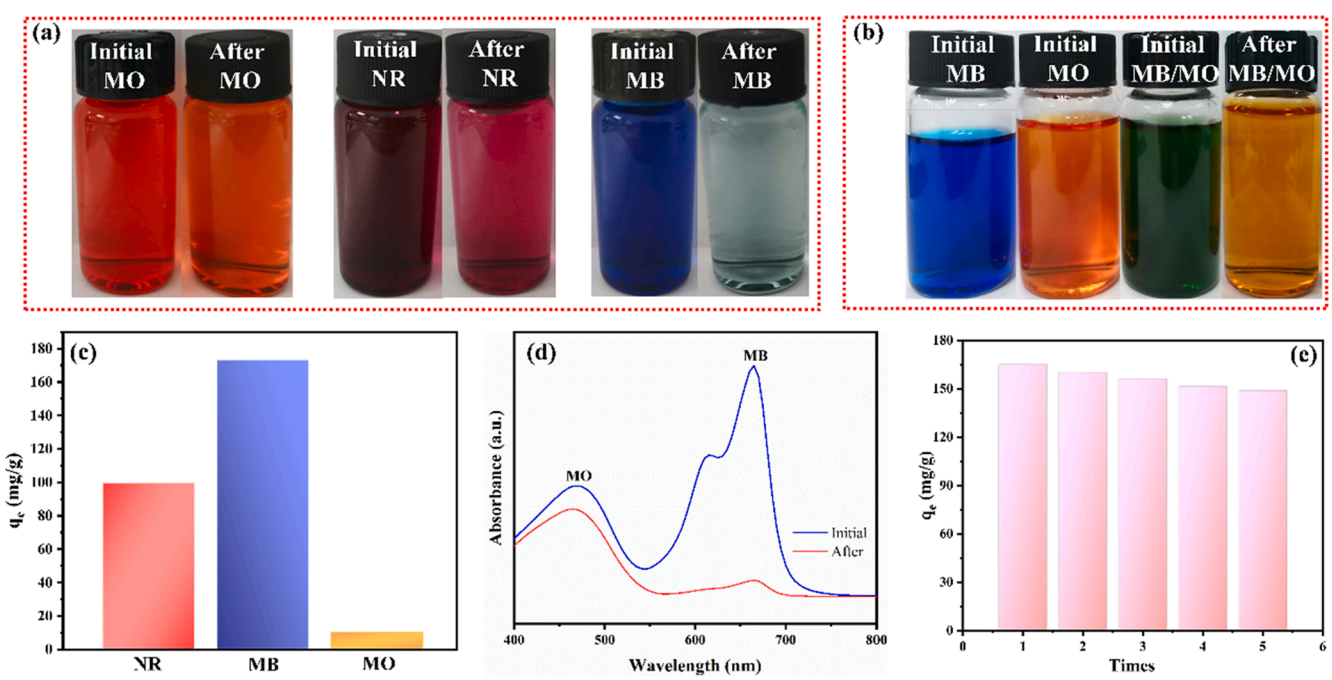

Fig. 5. (a) The photographs of three organic dye solutions including MO, NR and MB before and after adsorption by H-PDA-MCs. (b) The photograph of mixed dye solution of MB/MO before and after adsorption by H-PDA-MCs. (c) Equilibrium adsorption capacities of the H-PDA-MCs for three dyes: NR, MB and MO. (d) The UV–VIS absorption spectra of the mixed solutions of MB/MO before and after adsorption. (d) Reusability of H-PDA-MCs for capturing MB dye.

which can be validated by lightening the solution color after adsorption. Especially for MB dye, after adsorption the obtained dye solution was almost clear, implying that H-PDA-MCs own best uptake capacity towards cationic dye. This is also confirmed by the quantitative adsorption capacity measurement (Fig. 5c). Based on the fact that the surface of H-PDA-MCs is negatively charged under neutral conditions [40], and MO and MB are typical anionic dye and cationic dye respectively, we can speculate that H-PDA-MCs could preferentially capture cationic dye from mixed dye solution. To prove it, the binary mixed dye solution composing MB and MO was used to investigate the adsorption selectivity of H-PDA-MCs. As shown in Fig. 5b, the initial color of MB/MO mixed solution is cyan [37]. After adsorption by H-PDA-MCs, the mixed solution color displays orange, nearly the same as the color of single MO dye solution. And in the Fig. 5d, there are two strong absorption bands respectively corresponding the MB and MO in the absorption spectra of initial mixed solutions of MB/MO (blue line). After absorption, the absorption band assigned to the MB almost disappeared while that for the MO only exhibited a slight decline. This demonstrated that the H-PDA-MCs can selectively adsorb cationic dye from the mixed dye solution [41].

In addition, to check the cycle stability of H-PDA-MCs as adsorbent, the cyclic adsorption experiment was carried out using MB as adsorbate. In general, when the strong acids or bases can desorb the dye, it can be indicated that the absorption of the dye onto the adsorbent is by ion exchange or the electrostatic interaction [3]. Since H-PDA-MCs is negatively charged under neutral conditions and MB is a typical cationic dye, the adsorption of MB by H-PDA-MCs may be due to electrostatic interaction, so 1 M HCl solution was used as the desorption. As shown in Fig. 5e, the adsorption capacity of H-PDA-MCs gradually decreased with the number of cycles, but still kept over 84% after using five times, which indicates that due to ion exchange, MB could be largely eluted by HCl solution and H-PDA-MCs owned relatively good adsorption cycle stability [42]. At the same time, the phenomenon of incomplete desorption also indicates that there may be other interactions between H-PDA-MCs and MB besides electrostatic interaction. As the cycle time of adsorbent increases, the adsorption sites on the adsorbent gradually decrease as the eluent cannot completely elute MB, which is a reasonable reason why the adsorption efficiency decreases accordingly.

3.3. Kinetic studies

To explore the adsorption process of MB by H-PDA-MCs, the adsorption kinetics was studied using two common kinetic models as follows [43,44].

$$\text{Pseudo-first-order model}: ln(q_e - q_t) = ln(q_e) - K_1 t \quad (4)$$

$$\text{Pseudo-second-order model}: t / q_t = 1 / K_2 q_e^2 + t / q_e \quad (5)$$

where q_e (mg g^{-1}) and q_t (mg g^{-1}) represent the adsorption amount of H-PDA-MCs towards MB at equilibrium and at a given time, respectively. K_1 (min^{-1}) and K_2 (g mg^{-1} min^{-1}) represent pseudo-first-order rate

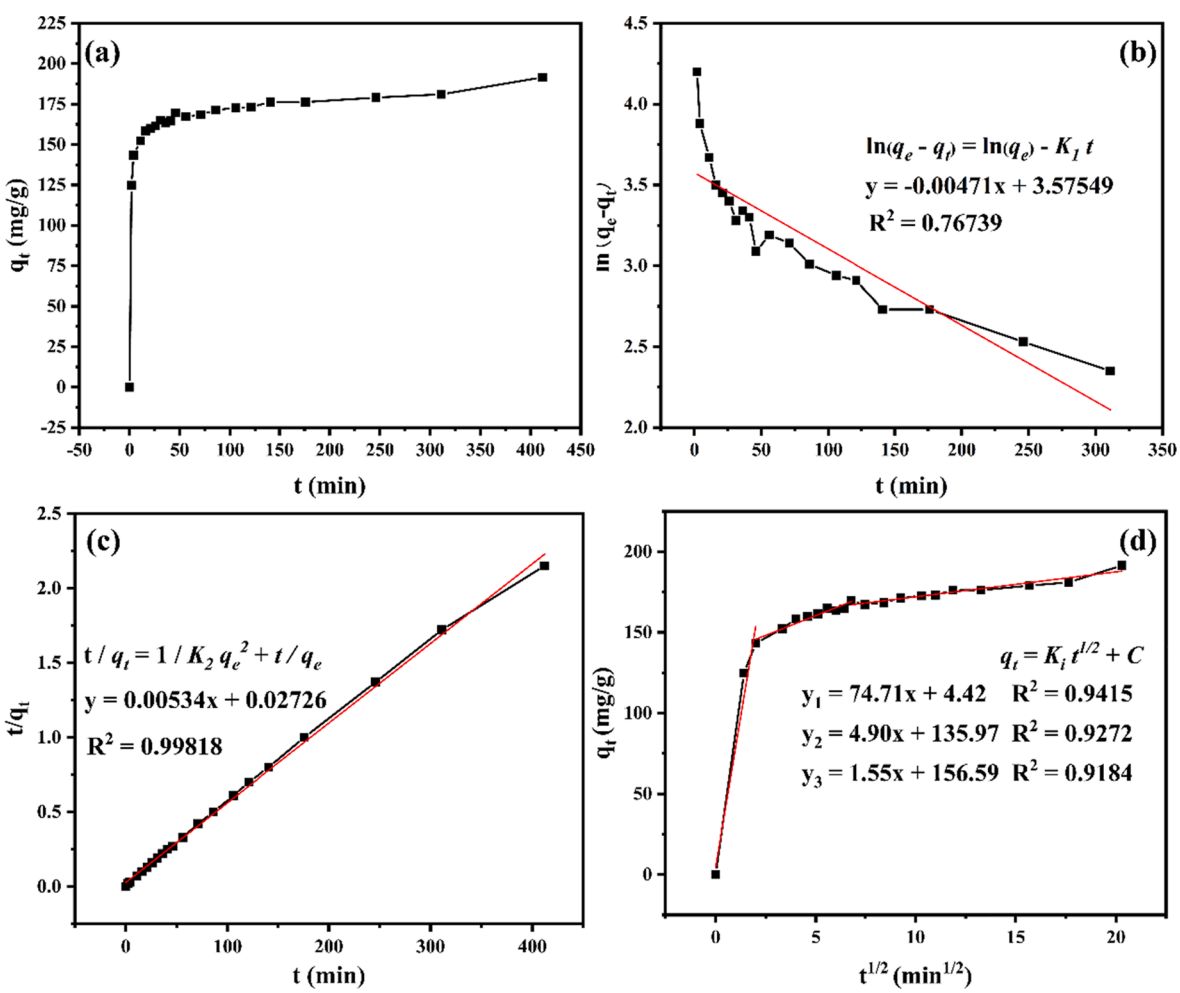

Fig. 6. (a) Effects of contact time on the adsorption of MB onto H-PDA-MCs. (Adsorption conditions: C_0 = 70 mg g^{-1}, m = 20 mg, V = 80 mL and T = 298.15 K). (b–d) Fitting plots of various kinetic models for MB adsorption by H-PDA-MCs: pseudo-first-order model (b), (c) pseudo-second-order model (c), and intraparticle diffusion (d).

constant and pseudo-second-order rate constant, respectively.

Fig. 6a depicts the influence of contact time on the adsorption capacity of H-PDA-MCs towards MB dye with the initial concentration of 70 mg L^{-1} at 25 °C. Obviously, the maximum adsorption capacity and the equilibrium time are 178.74 mg g^{-1} and 60 min, respectively. Compared with other micro/nano-scaled adsorbents (Table 1), the H-PDA-MCs exhibited high adsorption capacity and short equilibrium time (or rapid adsorption rate) significantly, indicating the hollow structure played a crucial role in enhancing the adsorption efficiency of an adsorbent. About the adsorption process of MB by H-PDA-MCs, the kinetic experiment data was further fitted based on pseudo-first-order model and pseudo-second-order model (Fig. 6b and c), and the corresponding kinetic parameters were calculated and listed in Table 2. By combining the figures and table, it can be found that the linear correlation coefficient (R^2 = 0.99818) of the pseudo-second-order kinetic fitting curve is much larger than that (R^2 = 0.76739) of the pseudo-first-order kinetic fitting curve. Furthermore, the value of $q_{e,cal}$ (187.27 mg g^{-1}) calculated in the pseudo-second-order model was more closer to the experimental value (178.74 mg g^{-1}), compared with the value of $q_{e,cal}$ (35.71 mg g^{-1}) calculated in the pseudo-first-order model. These results indicated that the adsorption process of MB onto H-PDA-MCs is suitable to be described by pseudo-second-order kinetics.

To thoroughly understand the adsorption mechanism and explore the rate-controlling steps in the adsorption process of MB by H-PDA-MCs, Weber-Morris intraparticle diffusion model was adopted and its formula is as follows (6) [5].

$$\text{Intraparticle diffusion model}: q_t = K_i t^{1/2} + C \tag{6}$$

where K_i (mg g^{-1} $min^{1/2}$) represents the intraparticle diffusion rate constant, and C (mg g^{-1}) is the intercept correlated with the adsorption stages.

Fig. 6d depicts the fitting curve of Weber-Morris intraparticle diffusion model for MB adsorption onto H-PDA-MCs, which can be divided into three straight lines corresponding to three adsorption stages [50]. The relevant parameters are calculated and summarized in Table 2. Evidently, and the intraparticle diffusion rate constants follow the order of $K_{i1} > K_{i2} > K_{i3}$. Among them, K_{i1} corresponds to the MB diffusion process from the bulk solution to the outside surface of H-PDA-MCs (first stage, film diffusion), K_{i2} is related to the intraparticle diffusion of MB molecules in the porous matrix of H-PDA-MCs (second stage, intraparticle diffusion), and K_{i3} corresponds to adsorption equilibrium (third stage). Based on the K_i value, we can conclude that the diffusion of MB molecules to the outer surface of H-PDA-MCs was a rapid process, followed by a slow process to the internal surface of H-PDA-MCs, and finally a tedious adsorption equilibrium [51,52]. Except that the third stage is a dynamic equilibrium, the second stage is an obvious key step determining the adsorption rate due to its lower K_i value. However, the fitting curve of the second stage does not across the origin, implying the intraparticle diffusion is not only a rate-limiting step [37]. The contribution of the boundary layer effect during the adsorption process can be reflected by the C value. Generally, a bigger C value corresponds to a greater contribution of the surface adsorption in the rate-limiting step. In this study, the larger C values suggest external mass diffusion of MB molecules onto H-PDA-MCs also played a significant role during the sorption process, especially in the initial sorption stage [33]. Additionally, the linear correlation coefficients of the three stages were in excess of 0.9, suggesting that Weber-Morris interparticle diffusion model is appropriate for studying the adsorption process of MB molecules on H-PDA-MCs.

Table 1
Comparison of adsorption capacities of different adsorbents for MB at 298.15 K.

Adsorbents	q_e (mg/g)	Refs.
Poly(cyclotriphosphazene-co-4,4′-sulfonyldiphenol) nanospheres	20.00	[25]
Carbon nanotubes	35.00	[45]
Multi-walled carbon nanotubes filled with Fe_2O_3 particles	42.00	[46]
Hollow PCPP microspheres	47.41	[20]
Poly(cyclotriphosphazene-co-4,4′-sulfonyldiphenol) nanotubes	69.16	[26]
Halloysite nanotubes	84.32	[47]
PDA microspheres	90.70	[33]
Palm kernel fiber	95.40	[48]
Magnetic γ-Fe_2O_3/SiO_2	116.10	[49]
H-PDA-MCs	178.74	This work

Table 2
Kinetic models for MB adsorption on H-PDA-MCs at 298.15 K.

Kinetic models	Model parameters	R^2
Pseudo-first order	$q_{e,cal}$ = 35.71 mg g^{-1} K_1 = −0.00471 min^{-1}	0.76739
Pseudo-second order	$q_{e,cal}$ = 187.27 mg g^{-1} K_2 = 0.00534 g mg^{-1} min^{-1}	0.99818
Intraparticle diffusion	K_{i1} = 74.7053 mg g^{-1} $min^{1/2}$ C_1 = 58.202 mg g^{-1}	0.9415
	K_{i2} = 1.638 mg g^{-1} $min^{1/2}$ C_2 = 155.174 mg g^{-1}	0.9272
	k_{i3} = 1.54503 mg g^{-1} $min^{1/2}$ C_3 = 1.54503 155.174 mg g^{-1}	0.9184

3.4. Adsorption isotherm studies

The research on equilibrium adsorption isotherm is of great significance for understanding the adsorbent-adsorbate interaction and designing a suitable adsorption system. First, the equilibrium adsorption experiments were carried out by varying solution temperature while keeping the adsorbent mass and dye concentration constant. Then, we checked the relationship between equilibrium concentration related to the initial concentration of the dye and equilibrium adsorption capacity of H-PDA-MCs. Five isotherm models, including Temkin, Langmuir, Freundlich, D-R (Dubnin-Radushkevich) and H-J (Harkins-Jura), were selected to fit the equilibrium experiment data of MB adsorption onto H-PDA-MCs. Of the five isotherm models, Langmuir model is based on a basic assumption that monolayer adsorption takes place at completely homogenous sites over the adsorbent surface. Freundlich model is suitable for describing a heterogeneous surface with non-uniform distribution of adsorption heat [53]. D-R model is usually used to distinguish the chemical or physical adsorption mechanism on the basis of a potential theory supposing heterogeneous surface [54]. Temkin model assumes that the adsorption heat (a function of temperature) of all the molecules in the adsorption layer could decrease linearly with the coverage due to the indirect adsorbent-adsorbent interaction [55]. H-J model considers multilayer adsorption and can be explained using the presence of a heterogeneous pore distribution [56]. The five isotherm equations (7-11) are given as follows [24,57,58].

$$\text{Temkin}: q_e = B_1 lnK_T + B_1 lnC_e \tag{7}$$

$$\text{Langmuir}: C_e/q_e = 1/(q_0 K_L) + (1/q_0)\, C_e \tag{8}$$

$$\text{Freundlich}: lnq_e = lnK_F + 1/n\, lnC_e \tag{9}$$

$$\text{Dubnin - Radushkevich}: lnq_e = lnq_0 - ß\, \varepsilon^2 \tag{10}$$

$$\text{Harkins - Jura}: 1/q_e = (B_2/A) - (1/A)\, lgC_e \tag{11}$$

where q_e (mg g^{-1}) is the amount of dyes adsorbed by H-PDA-MCs at equilibrium, B_1 is Temkin constant related to adsorption heat ($B_1 = RT/b$; T (K) is the absolute temperature, R (8.314 J mol^{-1} K^{-1}) is the universal gas constant), and K_T (L mg^{-1}) presents the equilibrium binding constant. C_e (mg L^{-1}) refers to the concentration of residual dye in the

solution at adsorption equilibrium. q_0 (mg g^{-1}) refers to the theoretical maximum capacity (monolayer saturation adsorption). K_L (L mg^{-1}) represents the Langmuir constant. K_F represents the Freundlich constant, n is the heterogeneity factor, β is *D-R* model constant (mol^2 kJ^{-2}). And ε refers to the polanyi potential and can be obtained by the formula of $\varepsilon = RT \ln(1 + 1/C_e)$. Finally, B_2 and A are the isotherm constants of H-J model.

The insert image in Fig. 7a shows the relationship between C_e and q_e. Obviously, the adsorption capacity of H-PDA-MCs increased with the augment of equilibrium concentration related to the initial concentration of the MB dye. High dye concentration can not only furnish more contact chance between dye molecules and active site of adsorbent but also supply strong driving force to overcome the resistance of mass transfer of dyes from aqueous phase to solid phases, and thus leading to the increase in dye uptake [59]. Fig. 7a–e give the linear fitting plots of the above five isotherm models for MB adsorption at the studied temperatures, respectively. And for each isotherm equation, the corresponding values of the constants and the correlation coefficient R^2 are calculated and summarized in Table 3. In these data obtained, it can be found that the values of R^2 in the case of Langmuir and Temkin models are significantly higher, which indicates that the two models are more suitable to describe the equilibrium adsorption than the other three ones. Of note, from the Langmuir isotherm data we can notice that the value of q_0 increases with temperature increase. And from the Temkin constant B_1, it is obvious that the adsorption heat increases with the rise of operating temperature. The two facts confirmed that the MB adsorption on H-PDA-MCs is endothermic.

In terms of Langmuir type adsorption process, R_L, a dimensionless constant separation factor, is often employed to evaluate if such adsorption process is favorable or unfavorable, and R_L value can be calculated from equation (12) [12].

$$R_L = 1 / (1 + K_L C_0) \tag{12}$$

where K_L (L mg^{-1}) is the Langmuir constant, and C_0 (mg L^{-1}) is the initial MB concentration. Generally, when R_L is equal to 0, between 0 and 1, equal to 1 or greater than 1, the adsorption process corresponds to irreversible, favorable, linear and unfavorable, respectively. It is obvious from Fig. 7f that the value of R_L is between 0.02 and 0.12, demonstrating that the MB adsorption on H-PDA-MCs is favorable.

Table 3
The isotherm constants and correlation coefficients of Temkin, Langmuir, Freundlich, D-R and H-J models.

Isotherm models	Parameters	T (K)		
		293.15	298.15	303.15
Temkin	K_T	0.0145	0.0143	0.0138
	B_1	188.9924	192.2894	197.8749
	R^2	0.9985	0.9987	0.9984
Langmuir	q_0	227.7904	233.1002	237.5297
	K_L	0.1524	0.1661	0.1929
	R^2	0.9986	0.9981	0.9990
Freundlich	K_L	119.7780	122.7071	132.7915
	1/n	8.1195	8.1096	8.8191
	R^2	0.9485	0.9084	0.9433
D-R	ß	4.3460	3.5717	2.7443
	q_0	204.1714	207.2281	214.6181
	R^2	0.6275	0.5848	0.6784
H-J	B_2	6.8932	4.9808	4.5802
	A	970.8738	641.0256	617.2840
	R^2	0.7613	0.7940	0.9391

3.5. Thermodynamic study

The thermodynamic parameters can be applied to assess the thermodynamic feasibility and the spontaneous nature of an adsorption process. In present study, the thermodynamic properties of MB dye adsorbed by H-PDA-MCs were studied by batch adsorption experiments in the temperature range of 298.15–318.15 K. The obtained experimental data were used to calculate the thermodynamic parameters including entropy change (ΔS^0), enthalpy change (ΔH^0), and free energy change (ΔG^0) according to the following equations (13) and (14).

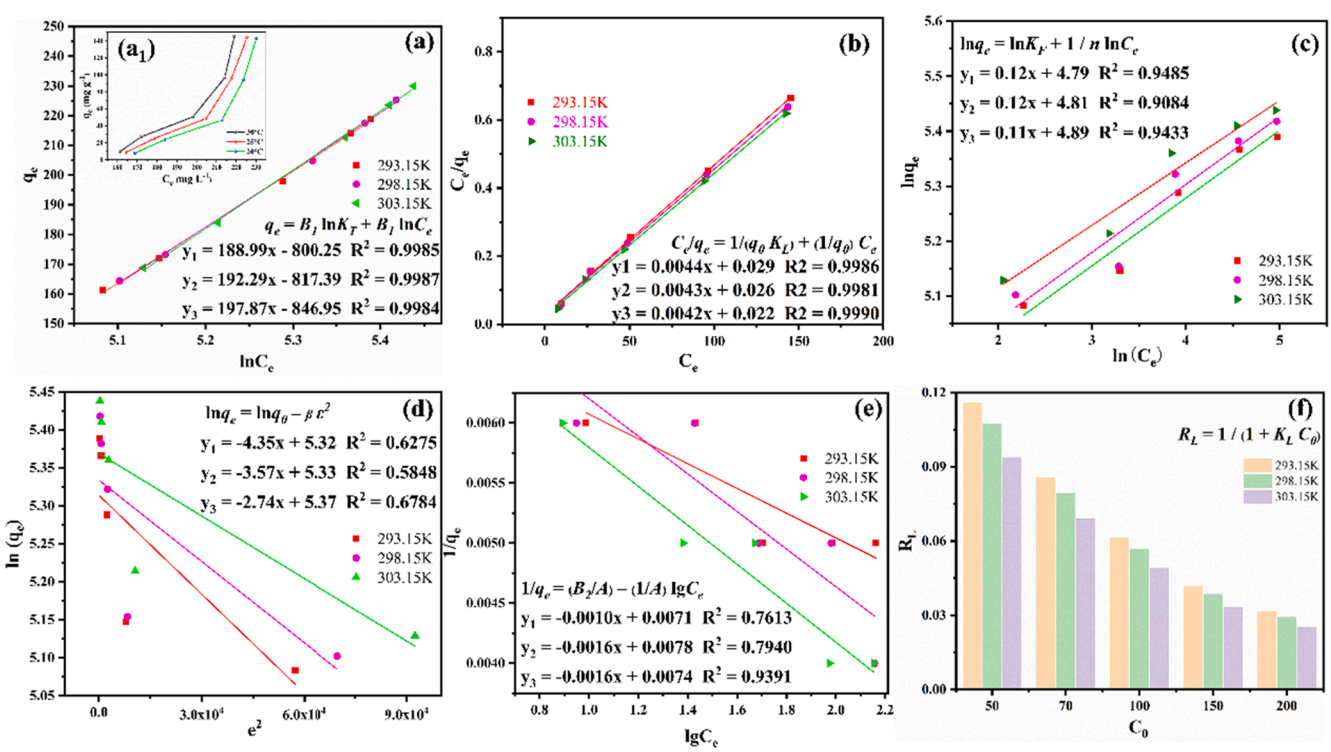

Fig. 7. (a) Temkin, (b) Langmuir, (c) Freundlich, (d) D-R, (e) H-J isotherms for the adsorption of MB onto the H-PDA-MCs at different temperatures. The insert image in (a) shows the relationship between C_e and q_e. (f) Separation factor R_L at different temperature and different initial concentrations.

$$\Delta G^0 = -RT\ lnK_0 \quad (13)$$

$$lnK_0 = \Delta S^0/R - \Delta H^0/(RT) \quad (14)$$

where K_0 is a dimensionless thermodynamic equilibrium constant ($K_0 = 55.5\ K_L$, herein, K_L is the Langmuir constant) [60], T (K) is the temperature in Kelvin, and R (8.314 J mol^{-1} K^{-1}) is the universal gas constant.

The Van't Hoff linear plot of the MB adsorption is shown in Fig. 8a. And from the image the values of ΔS^0 and ΔH^0 are determined according to the slope and intercept of the linear plot of lnK_0 versus $1/T$, respectively. The resultant thermodynamic parameters are listed in Fig. 8a (see insert table). Under the different temperature, ΔG^0 is always negative. This reveals that the adsorption process of MB dye by H-PDA-MCs is spontaneous in nature and thermodynamically feasible. When the operating temperature increases, the ΔG^0 value becomes smaller and smaller, implying that the high temperature is more advantageous to the MB adsorption. In Fig. 8a, the value of ΔH^0 is positive (17.35 KJ mol^{-1}), suggesting that the adsorption process is endothermic, hence, the adsorption capacity of H-PDA-MCs towards MB dye could rise with increasing operating temperature. This result is consistent with that shown in Fig. 4c and d. Additionally, the positive ΔS^0 value (76.82 J mol^{-1}) revealed that the randomness increased at the solid/liquid interface during the MB adsorption by H-PDA-MCs. This is a normal phenomenon for a physical adsorption process, which occurs through weak interactions. Finally, ΔG^0 values are negative and between 0 and −20, and the value of ΔH^0 is between 0 and 40, these indicate that the adsorption process of H-PDA-MCs removing MB is physical adsorption [24,32].

3.6. Study on adsorption mechanism

For investigating the adsorption mechanism, the FTIR spectrum contrast for H-PDA-MCs before and after MB adsorption was performed, and the results are shown in Fig. 8b. Evidently, after adsorption, the characteristic adsorption peak of MB appeared on the FTIR spectrum of H-PDA-MCs-MB, such as 578 cm^{-1} (frame vibration of C-S-C), 1770 cm^{-1} and 1714 cm^{-1} (stretching vibration of C═S) [61], implying that MB molecules have been captured successfully by H-PDA-MCs. Also, some absorption peaks of H-PDA-MCs-MB present an obvious redshift as follows. 1) The absorption peak of phenolic O-H at 3373 cm^{-1} was shifted to the low wave number (3353 cm^{-1}). We speculate that there was electrostatic interaction between the cationic dye MB molecule and the easily deprotonated phenolic O-H (negatively charged) on the adsorbent surface during the adsorption process. In other words, the phenolic O-H on H-PDA-MCs could make a great contribution for capturing MB molecules during the adsorption process. And such inference has a sufficient theoretical and experimental basis, which was analyzed in Fig. 4e and f. The adsorption capacity of H-PDA-MCs towards MB under alkaline condition was much larger than that under acidic condition. 2) The characteristic absorption peak of the aromatic ring was redshifted from 1611 cm^{-1} to 1597 cm^{-1}. The phenomenon was probably due to that both H-PDA-MCs adsorbent and MB adsorbate own planar six-membered ring structure, which were prone to form π-π

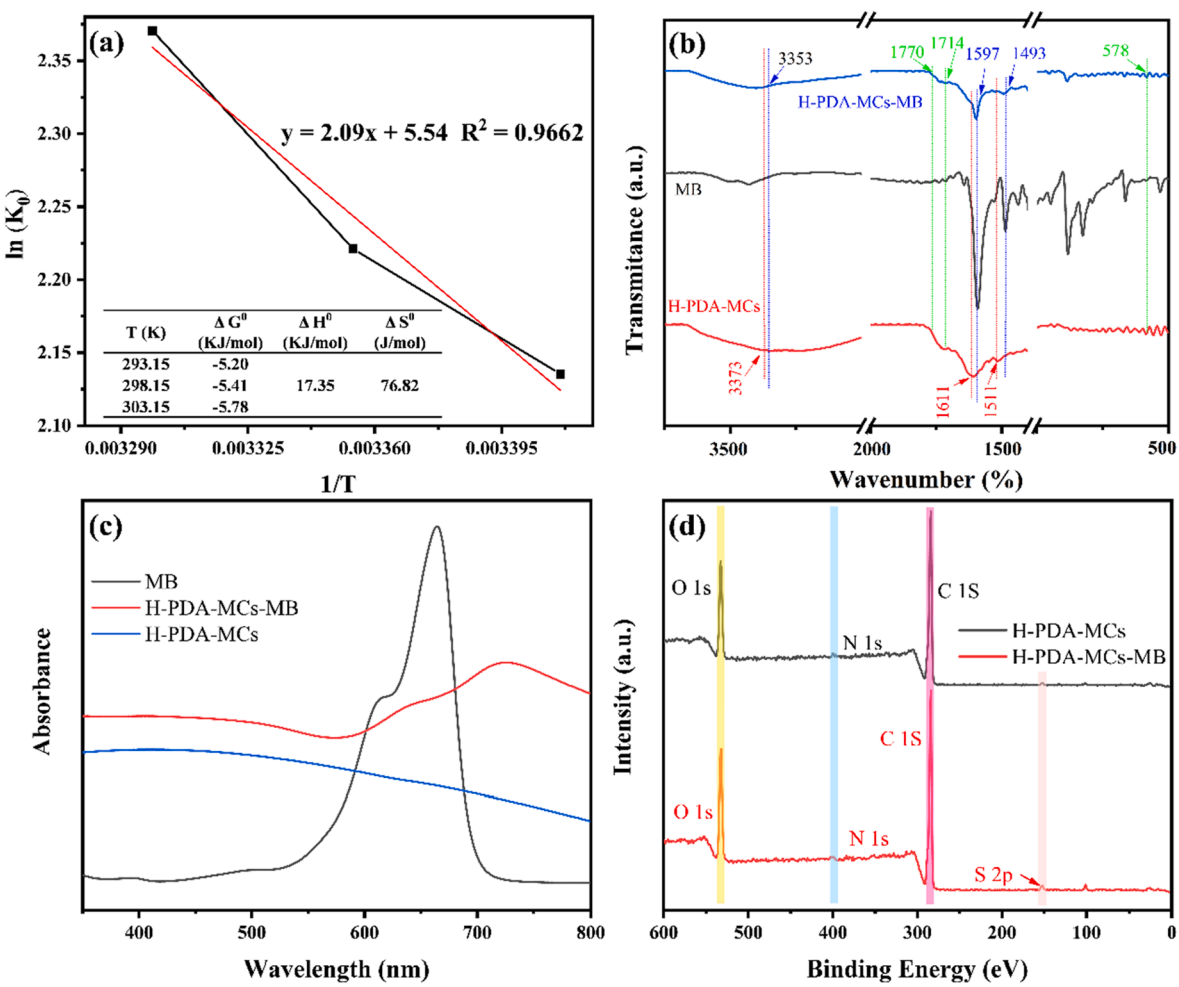

Fig. 8. (a) Regressions of Van't Hoff for thermodynamic and thermodynamic parameters. (b) FTIR spectra of MB, H-PDA-MCs, and H-PDA-MCs-MB. (c) UV–VIS adsorption spectra of MB, H-PDA-MCs, and H-PDA-MCs-MB. (d) XPS spectra of H-PDA-MCs and H-PDA-MCs-MB.

stacking effect between them. This corollary coincides with the experimental result (see Fig. 5a and c), where H-PDA-MCs could capture a large quantity of neutral dye NR with aromatic ring. Moreover, H-PDA-MCs could still adsorb a small amount of anionic dye MO with aromatic ring, though the electrostatic repulsion interaction produced between them at neutral solution circumstance. 3) The characteristic peak related to N-H shearing vibration in amine or imine groups was redshifted from 1511 cm^{-1} to 1493 cm^{-1}. It suggests that the hydrogen bonding could exist between H-PDA-MCs and MB molecules [30,62].

For further exploring the adsorption mechanism of organic dyes by H-PDA-MCs, the UV–VIS absorption spectra of H-PDA-MCs, MB and H-PDA-MCs-MB were measured. Fig. 8c shows that the characteristic peak of MB appears on the spectrum of H-PDA-MCs-MB. It indicates that MB is successfully adsorbed on the surface of H-PDA-MCs. In addition, the characteristic adsorption peak of MB in the H-PDA-MCs-MB spectrum appear an obvious bathochromic shift compared with that of pure MB. This is probably due to the interaction between H-PDA-MCs and MB (electrostatic interactions and π-π stack) [37]. And the result coincides with the infrared spectrum analysis above (Fig. 8b). Moreover, the results are consistent with the inferences of cyclic adsorption experiments.

X-ray photoelectron spectroscopy (XPS) is a good technique used to determine the surface chemical composition and elemental status in materials. Fig. 8d shows the comparison of XPS spectra before and after MB adsorption by H-PDA-MCs. It can be easily seen that a neonatal S 2p peak appears in the spectrum of H-PDA-MCs-MB compared with pure H-PDA-MCs. It indicates MB molecules were adsorbed on the surface of H-PDA-MCs. By fitting analysis of a single XPS spectrogram, the regions with the largest amount of information were C 1s, N 1s and O 1s regions. In the H-PDA-MCs, four peak components are fitted by the C 1s spectrum (Fig. 9a). The peak corresponding to aromatic C-H is the strongest with a value of 284.86 eV, followed by C-OH/C-N and C═O, whose peaks are 286.03 eV and 288.68 eV, respectively [63]. In addition, due to the π-π* transition in the aromatic ring, a low-intensity oscillation peak was located at 289.69 eV [64,65]. In the H-PDA-MCs-MB spectrum, the peak of π-π* disappeared (Fig. 9d), indicating the π-π interaction occurred between PDA and MB, which is completely consistent with the previous experimental result (Fig. 4e and f) and characterization result (Fig. 8b and c). Then, the two N 1s fitted peaks of H-PDA-MCs correspond to components of $-NH_2$ (400.57 eV) and -NH (399.40 eV) respectively (Fig. 9b). After adsorbing MB, the binding energy of $-NH_2$ increases, while that of -NH decreases (Fig. 9e). Meanwhile, the binding energy of both C═O (531.05 eV) and C-OH (533.16 eV) of H-PDA-MCs increased after adsorption of MB (Fig. 9c and f). Clearly, there are two reasons for this result. The first one is that there is hydrogen bonding between -NH of H-PDA-MCs and N of MB, and the second is that electrostatic interaction takes place between O^- of H-PDA-MCs and N^+ of MB [12,66–68]. Therefore, combining with the above experiments and characterization, we can draw a conclusion that the capture of cationic dye MB by H-PDA-MCs was mainly based on the mechanism of electrostatic interaction, hydrogen bonding and π-π stacking, as shown in Fig. 10.

4. Conclusions

In short, hollow PDA microcapsules were successfully synthesized by oxidation polymerization of dopamine using Fe_2O_3 nano-cube as template. The as-obtained H-PDA-MCs had hollow and mesoporous structure and large SSA (24.4 m^2 g^{-1}), and its surface was electronegative under neutral or alkaline conditions. The batch adsorption experiment results show that the adsorption capacity of H-PDA-MCs towards MB could be up to 191.55 mg g^{-1} and the adsorption equilibrium time is only 60 min at 298.15 K. Moreover, the H-PDA-MCs present excellent selective adsorption behavior towards cationic dye in binary mixed dyes. Kinetic studies display that the MB adsorption by H-PDA-MCs conforms to pseudo-second-order kinetic model. Based on the analysis of Weber-Morris intraparticle diffusion model, the adsorption process can be divided into three stages and the intraparticle diffusion is not the unique factor restricting the rate. Moreover, the adsorption isotherm consequences show that the adsorption follows the Temkin and Langmuir isothermal linear models. Adsorption thermodynamic data revealed that the adsorption process of H-PDA-MCs on MB was endothermic, spontaneous and thermodynamically feasible. The rapid, high-efficient and selective capture of H-PDA-MCs towards MB are based on

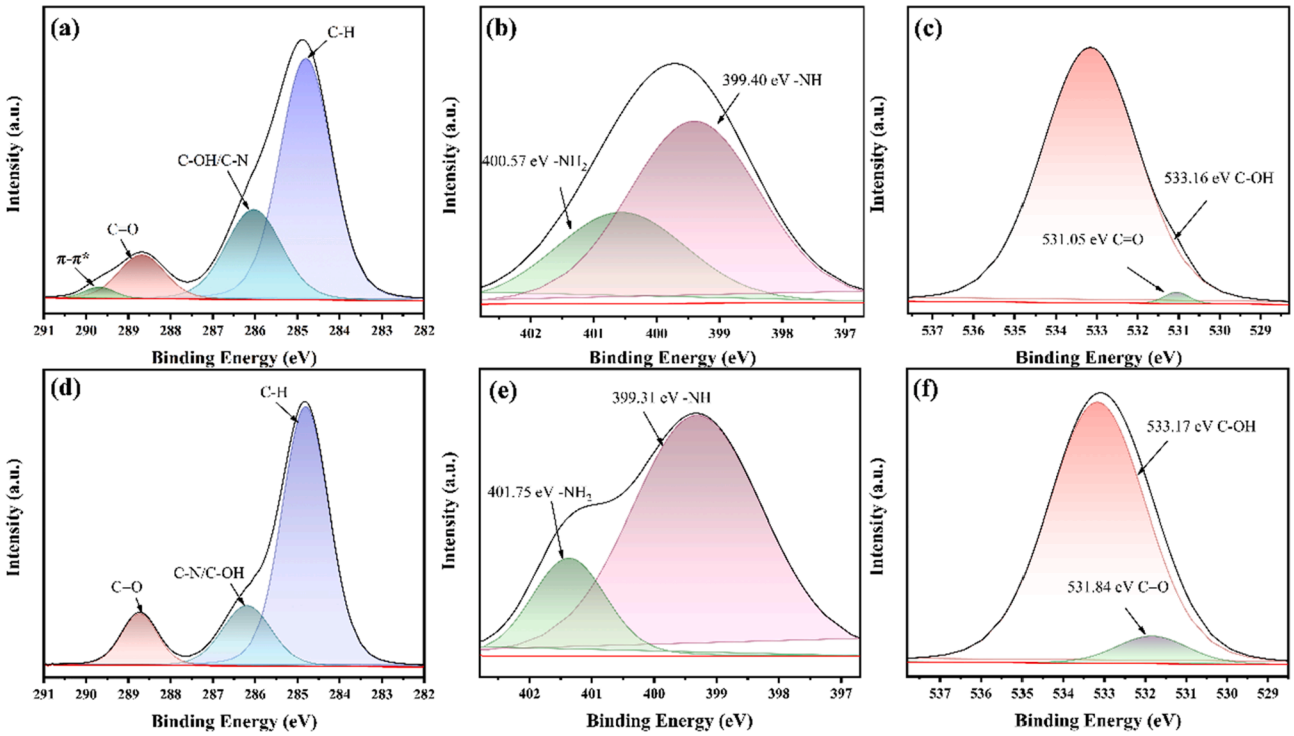

Fig. 9. (a–c) Peak-fitting XPS spectra of H-PDA-MCs: C 1s, N 1s and O 1s regions. (d–f) Peak-fitting XPS spectra of H-PDA-MCs-MB: C 1s, N 1s, O 1s regions.

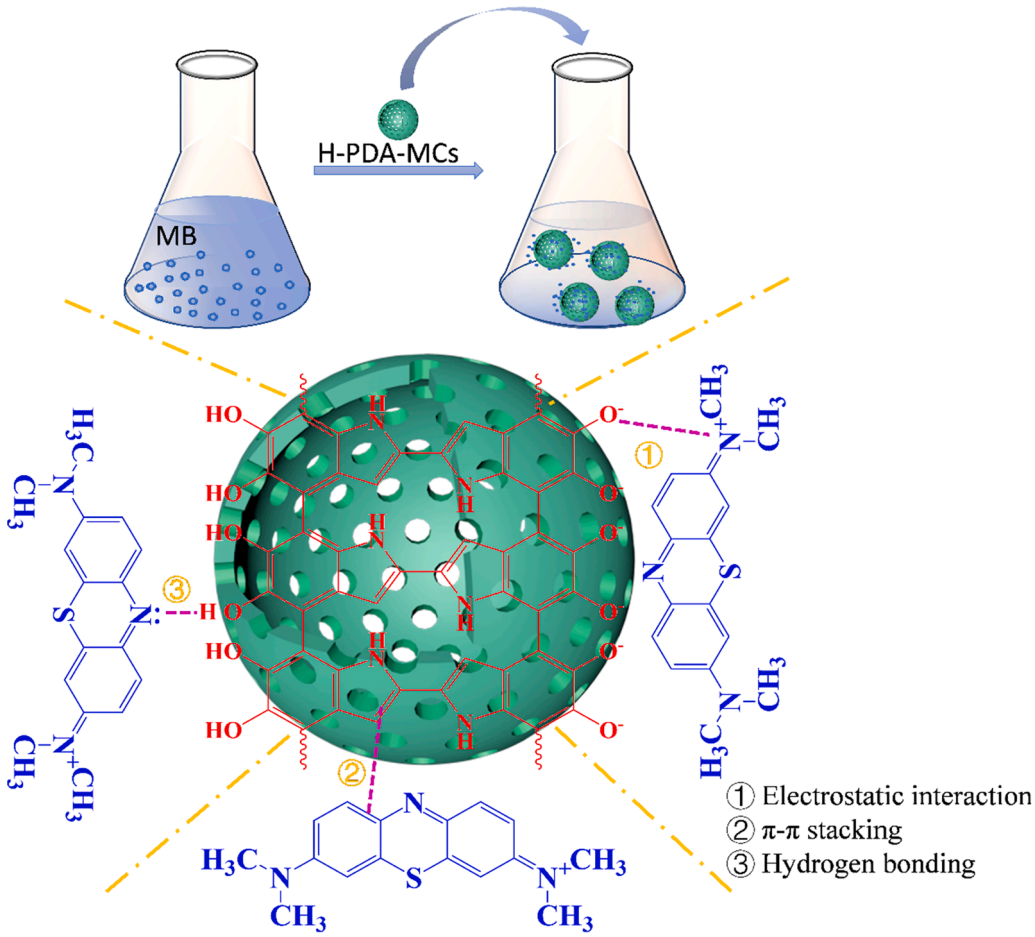

Fig. 10. Schematic illustration of the possible interaction mechanism between the H-PDA-MCs and MB.

multiple interactions including electrostatic interaction, hydrogen bonding and π-π stack. The study might offer a new idea for the structure design of new adsorbents with large adsorption capacity, high adsorption rate and good selective behavior.

CRediT authorship contribution statement

Mengling Feng: Conceptualization, Methodology, Software, Investigation, Writing - original draft. **Shichao Yu:** Validation, Formal analysis, Visualization, Software. **Pengchao Wu:** Validation, Formal analysis, Visualization. **Zhiwei Wang:** Validation, Formal analysis, Visualization. **Shaohua Liu:** Writing - review & editing. **Jianwei Fu:** Writing - review & editing.

Declaration of Competing Interest

The authors declare that they have no known competing financial interests or personal relationships that could have appeared to influence the work reported in this paper.

Acknowledgement

We are grateful to the National Natural Science Foundation of China (21101141), the Outstanding Young Talent Research Fund of Zhengzhou University (1521320002), the Natural Science Foundation of Henan (162300410252), and the Foundation for University Key Scientific Research of Henan Province of China (21A430036).

References

[1] F. Mashkoor, A. Nasar, Magsorbents: Potential candidates in wastewater treatment technology - A review on the removal of methylene blue dye, J. Magn. Magn. Mater. 500 (2020) 166408.
[2] K. Yamjala, M.S. Nainar, N.R. Ramisetti, Methods for the analysis of azo dyes employed in food industry - A review, Food Chem. 192 (2016) 813–824.
[3] J. Fu, J. Zhu, Z. Wang, Y. Wang, S. Wang, R. Yan, Q. Xu, Highly-efficient and selective adsorption of anionic dyes onto hollow polymer microcapsules having a high surface-density of amino groups: isotherms, kinetics, thermodynamics and mechanism, J. Colloid Interface Sci. 542 (2019) 123–135.
[4] A.M. Isloor, M.C. Nayak, B. Inamuddin, N. Prabhu, A.F. Ismail, A.M.A. Ismail, Novel polyphenylsulfone (PPSU)/nano tin oxide (SnO_2) mixed matrix ultrafiltration hollow fiber membranes: Fabrication, characterization and toxic dyes removal from aqueous solutions, React. Funct. Polym. 139 (2019) 170–180.
[5] O.A. Attallah, M.A. Al-Ghobashy, M. Nebsen, M.Y. Salem, Removal of cationic and anionic dyes from aqueous solution with magnetite/pectin and magnetite/silica/pectin hybrid nanocomposites: kinetic, isotherm and mechanism analysis, RSC Adv. 6 (2016) 11461–11480.
[6] Y. Feng, H. Zhou, G. Liu, J. Qiao, J. Wang, H. Lu, L. Yang, Y. Wu, Methylene blue adsorption onto swede rape straw (Brassica napus L.) modified by tartaric acid: equilibrium, kinetic and adsorption mechanisms, Bioresour. Technol. 125 (2012) 138–144.
[7] Y. He, G. Li, H. Wang, J. Zhao, H. Su, Q. Huang, Effect of operating conditions on separation performance of reactive dye solution with membrane process, J. Membr. Sci. 321 (2008) 183–189.
[8] G.M. Gadd, Biosorption: Critical review of scientific rationale, environmental importance and significance for pollution treatment, J. Chem. Technol. Biotechnol. 84 (2009) 13–28.
[9] C.A. Martinez-Huitle, E. Brillas, Decontamination of wastewaters containing synthetic organic dyes by electrochemical methods: a general review, Appl. Catal. B-Environ. 87 (2009) 105–145.
[10] S. Deng, H. Xu, X. Jiang, J. Yin, Poly(vinyl alcohol) (PVA)-enhanced hybrid hydrogels of hyperbranched poly(ether amine) (hPEA) for selective adsorption and separation of dyes, Macromolecules 46 (2013) 2399–2406.
[11] K. Yang, X. Li, J. Cui, M. Zhang, Y. Wang, Z. Lou, W. Shan, Y. Xiong, Facile synthesis of novel porous graphene-like carbon hydrogel for highly efficient

recovery of precious metal and removal of organic dye, Appl. Surf. Sci. 528 (2020) 146928.
[12] K. Wang, J. Fu, S. Wang, M. Gao, J. Zhu, Z. Wang, Q. Xu, Polydopamine-coated magnetic nanochains as efficient dye adsorbent with good recyclability and magnetic separability, J. Colloid Interface Sci. 516 (2018) 263–273.
[13] T.M.F. Marques, D.A. Sales, L.S. Silva, R.D.S. Bezerra, M.S. Silva, J.A. Osajima, O. P. Ferreira, A. Ghosh, E.C. Silva Filho, B.C. Viana, J.M.E. Matos, Amino-functionalized titanate nanotubes for highly efficient removal of anionic dye from aqueous solution, Appl. Surf. Sci. 512 (2020) 145659.
[14] G. Hong, M. Wang, X. Li, L. Shen, X. Wang, M. Zhu, B.S. Hsiao, Micro-nano structure nanofibrous p-sulfonatocalix[8]arene complex membranes for highly efficient and selective adsorption of lanthanum(III) ions in aqueous solution, RSC Adv. 5 (2015) 21178–21188.
[15] R. Gusain, N. Kumar, S.S. Ray, Recent advances in carbon nanomaterial-based adsorbents for water purification, Coordin. Chem. Rev. 405 (2020) 213111.
[16] B. Li, X. Jiang, J. Yin, Multi-responsive microgel of hyperbranched poly(ether amine) (hPEA-mGel) for the selective adsorption and separation of hydrophilic fluorescein dyes, J. Mater. Chem. 22 (2012) 17976–17983.
[17] X. Zheng, H. Zheng, Z. Xiong, R. Zhao, Y. Liu, C. Zhao, C. Zheng, Novel anionic polyacrylamide-modify-chitosan magnetic composite nanoparticles with excellent adsorption capacity for cationic dyes and pH-independent adsorption capability for metal ions, Chem. Eng. J. 392 (2020) 123706.
[18] Z.Y. Zhang, X.C. Xu, Wrapping carbon nanotubes with poly (sodium 4-styrenesulfonate) for enhanced adsorption of methylene blue and its mechanism, Chem. Eng. J. 256 (2014) 85–92.
[19] P. Zhang, J. Yin, X. Jiang, Hyperbranched poly(ether amine) (hPEA)/poly(vinyl alcohol) (PVA) interpenetrating network (IPN) for selective adsorption and separation of guest homologues, Langmuir 30 (2014) 14597–14605.
[20] J. Fu, Z. Chen, X. Wu, M. Wang, X. Wang, J. Zhang, J. Zhang, Q. Xu, Hollow poly (cyclotriphosphazene-co-phloroglucinol) microspheres: an effective and selective adsorbent for the removal of cationic dyes from aqueous solution, Chem. Eng. J. 281 (2015) 42–52.
[21] W.J. Lau, A.F. Ismail, Polymeric nanofiltration membranes for textile dye wastewater treatment: preparation, performance evaluation, transport modelling, and fouling control - A review, Desalination 245 (2009) 321–348.
[22] Y. Kotsuchibashi, M. Ebara, T. Aoyagi, R. Narain, Fabrication of doubly responsive polymer functionalized silica nanoparticles via a simple thiol-ene click chemistry, Polym. Chem. 3 (2012) 2545.
[23] S. Zhao, Y. Wen, C. Du, T. Tang, D. Kang, Introduction of vacancy capture mechanism into defective alumina microspheres for enhanced adsorption of organic dyes, Chem. Eng. J. 402 (2020) 126180.
[24] Q. Xin, J. Fu, Z. Chen, S. Liu, Y. Yan, J. Zhang, Q. Xu, Polypyrrole nanofibers as a high-efficient adsorbent for the removal of methyl orange from aqueous solution, J. Environ. Chem. Eng. 3 (2015) 1637–1647.
[25] Z. Chen, J. Fu, M. Wang, X. Wang, J. Zhang, Q. Xu, Adsorption of cationic dye (methylene blue) from aqueous solution using poly(cyclotriphosphazene-co-4,4'-sulfonyldiphenol) nanospheres, Appl. Surf. Sci. 289 (2014) 495–501.
[26] Z. Chen, J. Zhang, J. Fu, M. Wang, X. Wang, R. Han, Q. Xu, Adsorption of methylene blue onto poly(cyclotriphosphazene-co-4,4'-sulfonyldiphenol) nanotubes: kinetics, isotherm and thermodynamics analysis, J. Hazard. Mater. 273 (2014) 263–271.
[27] H. Lee, S.M. Dellatore, W.M. Miller, P.B. Messersmith, Mussel-inspired surface chemistry for multifunctional coatings, Science 318 (2007) 426–430.
[28] J. Liebscher, R. Mrowczynski, H.A. Scheidt, C. Filip, N.D. Hadade, R. Turcu, A. Bende, S. Beck, Structure of polydopamine: a never-ending story? Langmuir 29 (2013) 10539–10548.
[29] S. Kang, M. Baginska, S.R. White, N.R. Sottos, Core-shell polymeric microcapsules with superior thermal and solvent stability, ACS Appl. Mater. Interfaces 7 (2015) 10952–10956.
[30] K.X. Cui, B. Yan, Y.J. Xie, H. Qian, X.G. Wang, Q.X. Huang, Y.H. He, S.M. Jin, H. B. Zeng, Regenerable urchin-like Fe_3O_4@PDA-Ag hollow microspheres as catalyst and adsorbent for enhanced removal of organic dyes, J. Hazard. Mater. 350 (2018) 66–75.
[31] S. Liu, J. Pan, J. Cao, X. Dai, M. Meng, R. Wu, J. Yao, Y. Yan, Simultaneous removal of Pb(II) and 2,4,6-trichlorophenol by a hierarchical porous PU@PDA@MSNs sponge with reversible "shape memory" effect, Chem. Eng. J. 284 (2016) 10–20.
[32] K. Xu, J. Wu, Q. Fang, L. Bai, J. Duan, J. Li, H. Xu, A. Hui, L. Hao, S. Xuan, Magnetically separable h-Fe_3O_4@Au/polydopamine nanosphere with a hollow interior: a versatile candidate for nanocatalysis and metal ion adsorption, Chem. Eng. J. 398 (2020) 125571.
[33] J. Fu, Z. Chen, M. Wang, S. Liu, J. Zhang, J. Zhang, R. Han, Q. Xu, Adsorption of methylene blue by a high-efficiency adsorbent (polydopamine microspheres): kinetics, isotherm, thermodynamics and mechanism analysis, Chem. Eng. J. 259 (2015) 53–61.
[34] X.Y. Yu, H. Hu, Y.W. Wang, H.Y. Chen, X.W. Lou, Ultrathin MoS_2 nanosheets supported on N-doped carbon nanoboxes with enhanced lithium storage and electrocatalytic properties, Angew. Chem. Int. Ed. 54 (2015) 7395–7398.
[35] W. Lee, J.U. Lee, B.M. Jung, J.H. Byun, J.W. Yi, S.B. Lee, B.S. Kim, Simultaneous enhancement of mechanical, electrical and thermal properties of graphene oxide paper by embedding dopamine, Carbon 65 (2013) 296–304.
[36] X. Liu, J. Cao, H. Li, J. Li, Q. Jin, K. Ren, J. Ji, Mussel-inspired polydopamine: a biocompatible and ultrastable coating for nanoparticles in vivo, ACS Nano 7 (2013) 9384–9395.
[37] J. Fu, Q. Xin, X. Wu, Z. Chen, Y. Yan, S. Liu, M. Wang, Q. Xu, Selective adsorption and separation of organic dyes from aqueous solution on polydopamine microspheres, J. Colloid Interface Sci. 461 (2016) 292–304.
[38] Z. Cheng, Z. Wang, P. Wu, Y. Wang, J. Fu, Mass fabrication of oxygen and nitrogen co-doped 3D hierarchical porous carbon nanosheets by an explosion-assisted strategy for supercapacitor and dye adsorption application, Appl. Surf. Sci. 529 (2020) 147079.
[39] B. Chen, F. Long, S. Chen, Y. Cao, X. Pan, Magnetic chitosan biopolymer as a versatile adsorbent for simultaneous and synergistic removal of different sorts of dyestuffs from simulated wastewater, Chem. Eng. J. 385 (2020) 123926.
[40] F. Bernsmann, V. Ball, F. Addiego, A. Ponche, M. Michel, J.J. Gracio, V. Toniazzo, D. Ruch, Dopamine-melanin film deposition depends on the used oxidant and buffer solution, Langmuir 27 (2011) 2819–2825.
[41] L. Zhou, J. Huang, B. He, F. Zhang, H. Li, Peach gum for efficient removal of methylene blue and methyl violet dyes from aqueous solution, Carbohydr. Polym. 101 (2014) 574–581.
[42] S. Zeng, J. Tan, X. Xu, X. Huang, L. Zhou, Facile synthesis of amphiphilic peach gum polysaccharide as a robust host for efficient encapsulation of methylene blue and methyl orange dyes from water, Int. J. Biol. Macromol. 154 (2020) 974–980.
[43] M. Feng, W. You, Z. Wu, Q. Chen, H. Zhan, Mildly alkaline preparation and methylene bblue adsorption capacity of hierarchical flower-like sodium titanate, ACS Appl. Mater. Interfaces 5 (2013) 12654–12662.
[44] V.K. Gupta, A. Mittal, D. Jhare, J. Mittal, Batch and bulk removal of hazardous colouring agent Rose Bengal by adsorption techniques using bottom ash as adsorbent, RSC Adv. 2 (2012) 8381–8389.
[45] Y. Yao, F. Xu, M. Chen, Z. Xu, Z. Zhu, Adsorption behavior of methylene blue on carbon nanotubes, Bioresour. Technol. 101 (2010) 3040–3046.
[46] S. Qu, F. Huang, S. Yu, G. Chen, J. Kong, Magnetic removal of dyes from aqueous solution using multi-walled carbon nanotubes filled with Fe_2O_3 particles, J. Hazard. Mater. 160 (2008) 643–647.
[47] M. Zhao, P. Liu, Adsorption behavior of methylene blue on halloysite nanotubes, Microporous Mesoporous Mater. 112 (2008) 419–424.
[48] G.O. El-Sayed, Removal of methylene blue and crystal violet from aqueous solutions by palm kernel fiber, Desalination 272 (2011) 225–232.
[49] D. Chen, Z. Zeng, Y. Zeng, F. Zhang, M. Wang, Removal of methylene blue and mechanism on magnetic γ-Fe_2O_3/SiO_2 nanocomposite from aqueous solution, Water Resour. Ind. 15 (2016) 1–13.
[50] Y.M. Hao, C. Man, Z.B. Hu, Effective removal of Cu (II) ions from aqueous solution by amino-functionalized magnetic nanoparticles, J. Hazard. Mater. 184 (2010) 392–399.
[51] A.R. Bagheri, M. Ghaedi, A. Asfaram, R. Jannesar, A. Goudarzi, Design and construction of nanoscale material for ultrasonic assisted adsorption of dyes: application of derivative spectrophotometry and experimental design methodology, Ultrason. Sonochem. 35 (2017) 112–123.
[52] A.R. Bagheri, M. Ghaedi, A. Asfaram, S. Hajati, A.M. Ghaedi, A. Bazrafshan, M. R. Rahimi, Modeling and optimization of simultaneous removal of ternary dyes onto copper sulfide nanoparticles loaded on activated carbon using second-derivative spectrophotometry, J. Taiwan Inst. Chem. Eng. 65 (2016) 212–224.
[53] A. Kara, E. Demirbel, N. Tekin, B. Osman, N. Besirli, Magnetic vinylphenyl boronic acid microparticles for Cr(VI) adsorption: kinetic, isotherm and thermodynamic studies, J. Hazard. Mater. 286 (2015) 612–623.
[54] D. Kavitha, C. Namasivayam, Experimental and kinetic studies on methylene blue adsorption by coir pith carbon, Bioresour. Technol. 98 (2007) 14–21.
[55] F. Gimbert, N. Morin-Crini, F. Renault, P.M. Badot, G. Crini, Adsorption isotherm models for dye removal by cationized starch-based material in a single component system: error analysis, J. Hazard. Mater. 157 (2008) 34–46.
[56] N.K. Amin, Removal of direct blue-106 dye from aqueous solution using new activated carbons developed from pomegranate peel: adsorption equilibrium and kinetics, J. Hazard. Mater. 165 (2009) 52–62.
[57] A.S. Bhatt, P.L. Sakaria, M. Vasudevan, R.R. Pawar, N. Sudheesh, H.C. Bajaj, H. M. Mody, Adsorption of an anionic dye from aqueous medium by organoclays: equilibrium modeling, kinetic and thermodynamic exploration, RSC Adv. 2 (2012) 8663–8671.
[58] F.F. Ma, D. Zhang, N. Zhang, T. Huang, Y. Wang, Polydopamine-assisted deposition of polypyrrole on electrospun poly(vinylidene fluoride) nanofibers for bidirectional removal of cation and anion dyes, Chem. Eng. J. 354 (2018) 432–444.
[59] Y. Song, Y. Duan, L. Zhou, Multi-carboxylic magnetic gel from hyperbranched polyglycerol formed by thiol-ene photopolymerization for efficient and selective adsorption of methylene blue and methyl violet dyes, J. Colloid Interface Sci. 529 (2018) 139–149.
[60] Y. Liu, Is the free energy change of adsorption correctly calculated? J. Chem. Eng. Data 54 (2009) 1981–1985.
[61] N.X. Gui, S.Q. Man, Surface enhenced Raman scattering of methylene blue adsorbed on capshaped siver nanoparticles, Chem. Phys. Lett. 447 (2007) 322–327.
[62] L. Ai, C. Zhang, F. Liao, Y. Wang, M. Li, L. Meng, J. Jiang, Removal of methylene blue from aqueous solution with magnetite loaded multi-wall carbon nanotube: kinetic, isotherm and mechanism analysis, J. Hazard. Mater. 198 (2011) 282–290.
[63] M.B. Clark Jr., M.B. Clark Jr., T.M. Schultz, D.G. Patil, L. Salvati Jr., Solid-state analysis of eumelanin biopolymers by electron spectroscopy for chemical analysis, Anal. Chem. 62 (1990) 949–956.
[64] I. Kaminska, M.R. Das, Y. Coffinier, J. Niedziolka-Jonsson, J. Sobczak, P. Woisel, J. Lyskawa, M. Opallo, R. Boukherroub, S. Szunerits, Reduction and functionalization of graphene oxide sheets using biomimetic dopamine derivatives in one step, ACS Appl. Mater. Interfaces 4 (2012) 1016–1020.
[65] E.S.C. Jones, The effect of low power plasmas on carbon fibre surfaces, Carbon 28 (1990) 509–514.

[66] N.M. Mackie, D.G. Castner, E.R. Fisher, Characterization of pulsed-plasma-polymerized aromatic films, Langmuir 14 (1998) 1227–1235.
[67] B. Chen, Y. Cao, H. Zhao, F. Long, X. Feng, J. Li, X. Pan, A novel Fe^{3+}-stabilized magnetic polydopamine composite for enhanced selective adsorption and separation of Methylene blue from complex wastewater, J. Hazard. Mater. 392 (2020) 122263.
[68] K. Gupta, O.P. Khatri, Fast and efficient adsorptive removal of organic dyes and active pharmaceutical ingredient by microporous carbon: effect of molecular size and charge, Chem. Eng. J. 378 (2019) 122218.